# OH observations of space shuttle exhaust

Michael H. Stevens and Christoph R. Englert
E.O. Hulburt Center for Space Research, Naval Research Laboratory, Washington, DC, USA

Jörg Gumbel
Universities Space Research Association, Washington, DC, USA

Received 8 March 2002; accepted 5 April 2002; published 21 May 2002.

[1] We report the unexpected observation of a large hydroxyl (OH) cloud north and east of the United States a day after a space shuttle launch in November, 1994. The Middle Atmosphere High Resolution Spectrograph Investigation (MAHRSI) observed OH(0,0) solar fluorescence near 309 nm while staring toward a tangent altitude of 87 km, where OH can be produced from water vapor photodissociation. The OH(0,0) band has a rotational temperature of 252 ± 23 K corresponding to an altitude of 110 ± 3 km, where nearly half of the shuttle's main engine water vapor exhaust is released on ascent. The location of the cloud one day after injection into the atmosphere implies that its average velocity is between 26–40 m/s northward. We also report strong evidence of water ice measured simultaneously along the same line of sight, suggesting that water vapor exhaust is redistributed by condensation and sedimentation. *INDEX TERMS:* 0305 Atmospheric Composition and Structure: Aerosols and particles (0345, 4801); 0341 Atmospheric Composition and Structure: Middle atmosphere—constituent transport and chemistry (3334); 0355 Atmospheric Composition and Structure: Thermosphere—composition and chemistry; 0360 Atmospheric composition and structure: Transmission and scattering of radiation

## 1. Introduction

[2] The impact of rocket exhaust on the upper atmosphere was a topic of intense research in the late 20th century [*Kellogg*, 1964; *Forbes*, 1980; *Mendillo*, 1988]. However, there is still little data to provide insight to the ultimate fate of the effluents. Direct measurements are limited to either the stratosphere [e.g. *Newman et al.*, 2001; *Ross et al.*, 2000] or to altitudes near 300 km [e.g. *Murad et al.*, 1990; *Bernhardt et al.*, 1998]. More indirect measurements do not have the altitude resolution for quantitative analysis [*Kozlov and Smirnova*, 1998].

[3] The propellant combination used by the space shuttle's main engines is liquid oxygen and liquid hydrogen, which produce 96.6% water vapor by weight [*AIAA*, 1991]. Much of it is injected into the lower thermosphere so that observation of this water vapor in the hours and days after launch can yield information on not only its fate but also on lower thermospheric dynamics. Above ~65 km, OH is produced primarily from water vapor photodissociation by solar ultraviolet radiation so that OH inferred at these altitudes can be used as a proxy for water vapor.

[4] Here we report the observation of a large OH cloud a day after launch of the space shuttle (STS-66) in November 1994, while staring at a tangent altitude of 87 km. When viewing the limb detected emissions can originate from anywhere along the line of sight, so the cloud can be higher than 87 km. We further constrain its altitude by the OH rotational emission temperature and knowledge of the vertical temperature structure in November. We also report the simultaneous observation of enhanced scattered sunlight along the same line of sight, most likely due to water ice. The ultimate fate of the shuttle's main engine exhaust as well as possible implications to the water budget of the middle atmosphere are briefly discussed in the context of these new and unexpected observations.

## 2. The Observations

[5] On November 3rd, 1994 at 16:59:43 UT STS-66 was launched from the Kennedy Space Center carrying the Cryogenic Infrared Spectrometers and Telescopes for the Atmosphere-Shuttle Pallet Satellite (CRISTA-SPAS). Figure 1 shows the ground track of the shuttle in red for the first nine minutes of flight. CRISTA-SPAS was deployed 20 hours later at an altitude near 317 km and an orbital inclination of 57°. MAHRSI was aboard CRISTA-SPAS and on its first of two shuttle missions to observe OH and nitric oxide in the Earth's middle atmosphere.

[6] MAHRSI measured solar resonance fluorescence of the OH $A^2\Sigma^+ - X^2\Pi$ (0,0) band near 309 nm at a spectral resolution of 0.02 nm by viewing the Earth's limb. The line of sight was directed to a tangent altitude in the antivelocity direction and 18° above the orbital plane. Figure 1 shows that 26 hours after launch, MAHRSI

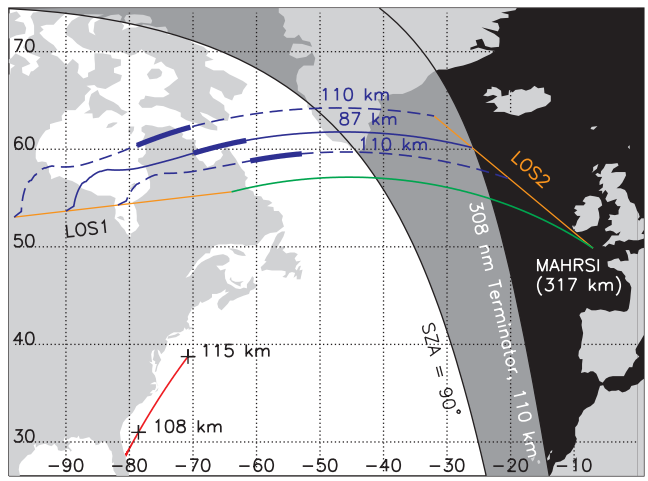


**Figure 1.** Map showing the geographic region relevant to this work. The red line shows the ground track of STS-66 for the nine minutes following launch. Between 108–115 km altitude about 300 metric tons of water vapor were released into the atmosphere. The green line is the MAHRSI ground track 26 hours after launch, the solid blue line is the ground track of the tangent point and the dashed blue lines are the near and far field ground tracks at 110 km. OH spectra and enhanced solar scattering were unambiguously measured between line of sight 1 (LOS1) and line of sight 2 (LOS2). The thick blue lines show where the OH rotational temperature is inferred from the data.


0094-8276/02/2002GL015079$05.00

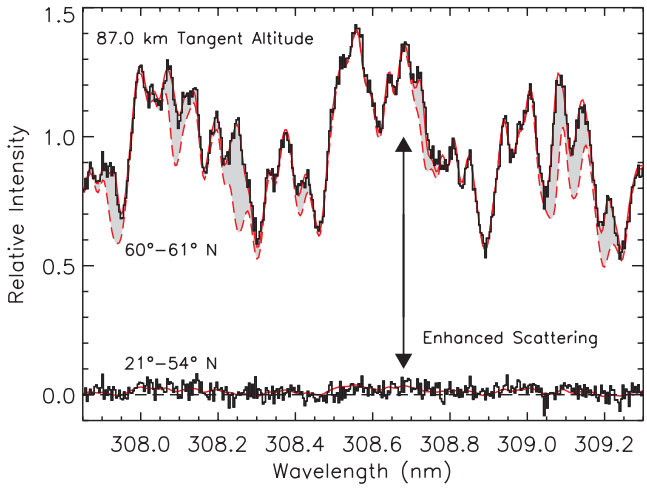


**Figure 2.** The averaged limb spectrum staring toward a tangent altitude of 87 km early in the orbit is shown as the lower histogram (11 minutes of integration time). Shown as the upper histogram is a limb spectrum obtained from the highlighted region in Figure 1 (1.1 minutes) with greatly enhanced OH emission and scattered ultraviolet sunlight. The heavy red line is the modeled limb spectrum, the dashed line is the fitted background and the shaded area is the inferred OH signal. The two MARHSI limb spectra are measured staring toward the same tangent altitude.

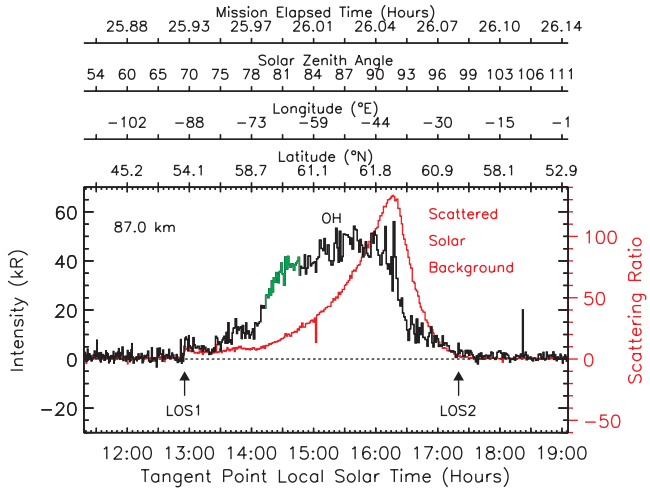


**Figure 3.** Observations of OH radiances (black histogram) and scattering ratios (red histogram) as a function of local time. The time period over which temperature is inferred is highlighted in green and the corresponding geographic region is shown in Figure 1.

was just south of Greenland at high northern latitudes. MAHRSI was staring at a fixed tangent altitude of 87.0 km, where OH is normally below MAHRSI's detection threshold and the solar (Rayleigh) scattered background is very weak. However, starting abruptly at 18:55:19 UT, MAHRSI simultaneously measured OH emission and enhanced scattered sunlight for 8.9 minutes. A portion of these spectra are averaged and shown in the upper histogram of Figure 2.

[7] Each 2.2 s limb spectrum is fit using a non-linear least squares fitting algorithm that includes the background spectral shape, a theoretical OH spectrum, a constant and a first-degree polynomial. The shaded area in Figure 2 shows the OH(0,0) emission envelope on top of the solar scattered background. The complex shape of the background is well understood and has been used to retrieve weaker OH(0,0) intensities in previous studies [e.g. *Conway et al.*, 1999].

[8] Comparison of the dramatically different limb spectra from the dayside of the same orbit in Figure 2 shows that the difference is not due to Rayleigh scattering from the ambient atmosphere. It is also not due to Rayleigh scattering from a cloud of pure water vapor since water vapor's Rayleigh scattering cross section is comparable to that of dry air at 309 nm [*Bodhaine et al.*, 1999]. Since the enhanced scattering is measured simultaneously and along the same line of sight as the OH, the background in Figure 2 is most likely due to water ice particles [*Stevens et al.*, 2001].

## 3. Data Analysis

### 3.1. The Exhaust Trail

[9] Figure 3 shows the OH band intensity integrated over the 11 brightest emission features between 307.8 and 310.6 nm [*Conway et al.*, 1999] as a function of local time (LT). Shown on the top axes are the tangent point latitude, longitude, solar zenith angle (SZA) and mission elapsed time. Note that the geographic region and lighting conditions are slightly different for emissions originating from the near or far field along the line of sight (Figure 1). The peak intensity in Figure 3 is 56 ± 9 kR which yields an OH column abundance of 2.1 ± 0.4 × $10^{14}$ $cm^{-2}$ using the *g*-factor for the 11 brightest features [*Stevens and Conway*, 1999].

[10] Figure 3 also shows that OH and ice were always detected simultaneously during these observations. Shown on the right hand axis of Figure 3 are scattering ratios for the ice. The "clear air" scattering ratio was calculated by averaging the limb intensities between 11.3–12.9 LT.

### 3.2. The OH Emission Temperature

[11] Although information on the vertical distribution of OH is limited due to the fixed line of sight, the OH emission altitudes may be inferred from the OH rotational temperature. The relative intensities of the individual rotational lines are determined by temperature dependent Boltzmann statistics [*Stevens and Conway*, 1999]. Figure 4 shows an average OH spectrum from the limb spectrum in Figure 2. The two features in Figure 4 are made up of five different rotational lines. Near 308.42 nm are two lines originating from transitions at a higher rotational level ($N'' = 4$) than the three near 308.25 nm so that the 308.42 nm feature brightens relative to 308.25 nm with increasing temperature. Intensities are inferred from the data by summing the middle 11

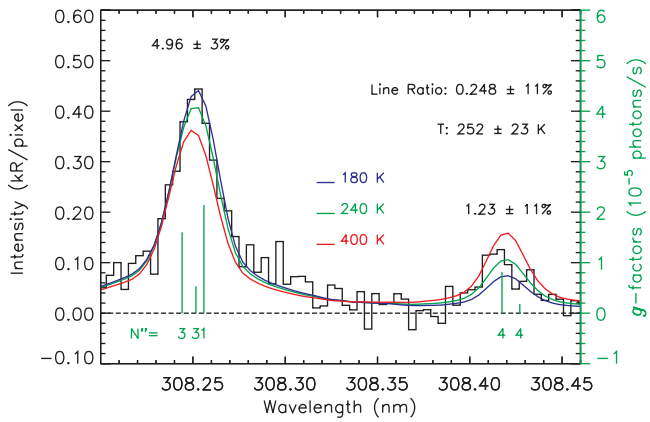


**Figure 4.** The OH spectrum from the difference of the limb spectrum and the fitted background in Figure 2. Rotational *g*-factors at 240 K are labeled in green and the temperature is determined from the ratio of the two features shown.

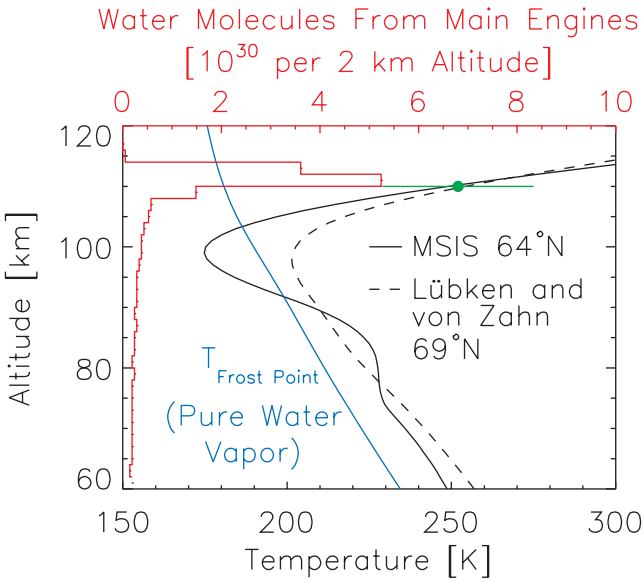


**Figure 5.** Ambient temperature profiles (black) and the frost point temperature (blue) for pure water vapor. The plume altitude inferred from the OH rotational emission temperature is also indicated in green. The red histogram referenced to the top axis shows the amount of water vapor injected into 2 km layers of the atmosphere by the shuttle.

pixels in each feature and scaling that to infer the total emission. This scale factor is between 1.5–1.6 and calculated by convolving a theoretical *g*-factor spectrum with MAHRSI spectral resolution functions [*Conway et al.*, 1999].

[12] Figure 4 also shows modeled spectra at three different temperatures scaled to fit the OH data. We infer a temperature of 252 ± 23 K from the ratio of the two features shown. Figure 5 shows that this temperature corresponds to an altitude of 110 ± 2 km using an MSIS-90 temperature profile [*Hedin*, 1991] or 110 ± 3 km using an Arctic climatology [*Lübken and von Zahn*, 1991]. Figure 5 also shows the amount of water vapor injected into the atmosphere by the shuttle as a function of altitude in red. Of the $2.2 \times 10^{31}$ molecules of water vapor released by the main engines from launch to orbit, 44% are injected into a narrow altitude region between 108–114 km. This altitude region is in remarkable agreement with that inferred from the OH spectrum in Figure 4 and indicates that the OH observed at high latitudes 26 hours after launch is from photodissociated water vapor injected into the atmosphere by the shuttle.

### 3.3. The OH Concentration in the Plume

[13] At 110 km altitude, results from a one-dimensional photochemical model [*Summers et al.*, 1997] show that the solar irradiance between 130–175 nm dominates the photodissociation of water vapor with Ly-α near 121.6 nm also contributing. By simulating the lighting conditions of the plume from the release point near 35° N to the observations near 60° N a day later, we find that photodissociation depletes the water vapor by only 30%. This calculation does not include opacity to Ly-α by water vapor itself, which is not negligible and would result in even less depletion after a day.

[14] Following the injection of the water vapor exhaust, the plume expands to a diameter of ~3 km to reach equilibrium with the ambient pressure near 110 km altitude. Slower diffusion and mixing processes determine the further spatial development of the plume [*Vlasov and Grushin*, 1996]. Model results of a 2 km layer of pure water vapor at 110 km yield a local OH density of $1.0 \times 10^9$ cm$^{-3}$ for the late afternoon conditions of our observations (16:00 local time, 60° N). With the observed OH column number density $2.1 \times 10^{14}$ cm$^{-2}$ inferred from our data (section 3.1) this yields a path length of 2.1 km, very close to the ~3 km plume diameter inferred above, given uncertainties in the orientation of the line of sight through the plume.

[15] A Russian Proton rocket with a propellant combination of $N_2O_4$/UDMH (Unsymmetrical Dimethylhydrazine) was launched from the Baikonur Cosmodrome in Tyuratam, Kazakhstan (48° N, 63° E) four days prior to our observations. Although its effluents could have conceivably ended up in our line of sight, the amount of fuel is about half of that in the shuttle, water vapor only constitutes 46% of the $N_2O_4$/UDMH products [*AIAA*, 1991] and photodissociation would have reduced the amount of water vapor present by an additional factor of three over four days. As a result, the diffused plume would have about 13 times less water vapor present assuming that the launch trajectory convolved with the wind fields brought the plume to our point of observation. We regard this as a possible but very unlikely scenario.

## 4. Discussion

[16] The implications for the transport of shuttle exhaust near 110 km are evident from the high latitude of the observation. The required northward transport speed of the cloud from its injection between 31–38° N to its northernmost point of observation between 60–64° N is 26–40 m/s. Although these velocities are higher than average meridional winds predicted by a general circulation model [*Roble and Ridley*, 1994], observations by the High Resolution Doppler Imager indicate that average northward winds in the winter near 105 km can exceed 20 m/s [*Lieberman et al.*, 2000].

[17] If the exhaust continues on a path into the polar night (~75° N in early November), photodissociation is cut off and water vapor could be transported downward to the middle atmosphere where chemical lifetimes are generally much longer [*Körner and Sonnemann*, 2001]. The rapid meridional circulation indicated by our observations would necessarily be accompanied by rapid downward motion near the pole.

[18] If the plume does not reach the polar night, the ice offers another means of transport down to the middle atmosphere. Note from Figure 5 that the frost point for pure water vapor at ambient pressure is 181 K at 110 km [*Marti and Mauersberger*, 1993]. Although this is at least 48 K below the inferred OH rotational temperature the frost point is reached at 103 km for the MSIS profile, where the shuttle also left appreciable amounts of water vapor. Since we do not know at what altitude (above 87 km) the solar scattering from ice originates and we do not have quantitative data on the atmospheric temperature variability, we cannot provide an explanation on how and where the ice forms or on the particle size distribution.

[19] If the exhaust from a single shuttle launch was transported down to the upper mesosphere, locally enhanced concentrations there are possible. It is interesting to note that a large cloud of water vapor was inferred from MAHRSI OH observations between 72–80 km altitude east of the United States and 3–4 days after launch of STS-66 [*Conway et al.*, 1999]. This is south of the observations presented here but near the inferred path of the plume. The cloud measures about 14° latitude by 120° longitude and contributes to the pronounced upper mesospheric water vapor layer reported by *Summers et al.* [1997] and discussed by *Summers and Siskind* [1999]. If all of the STS-66 exhaust injected between 108–114 km altitude formed ice, fell, and sublimated without loss at 70 km, the zonally averaged water vapor concentration would be increased by ~0.03 ppmv or ~3% of the observed layer. This is small but worthy of consideration given that contributions from other launches are not included here. The fate of shuttle exhaust for a summer launch will be

discussed in future work with observations from the second MAHRSI mission in August, 1997.

## 5. Summary

[20] We infer a large cloud of water vapor at 110 ± 3 km altitude from MAHRSI OH observations north and east of the United States one day after launch of STS-66. We show that this cloud is at the same altitude as an extended trail of water vapor exhaust released from the shuttle's main engines less than ten minutes after launch. Average northward transport speeds of the plume are between 26–40 m/s. If the cloud reaches the polar night, photodissociation stops and downward circulation can bring the water vapor to the middle atmosphere where chemical lifetimes are longer. Our simultaneous observations of ice along the same line of sight suggest a second means of transport down to the middle atmosphere through condensation, sedimentation and sublimation.

[21] More synoptic observations of launch vehicle exhaust are required to better understand the fate of water within the plumes in the upper mesosphere and lower thermosphere. For example, it is not known from our observations whether water vapor released at low latitudes in the lower thermosphere can enter the polar night so that its distribution is controlled by downward transport. Observations of OH, water vapor and ice would provide important information on the possible redistribution of water vapor exhaust. Because the upper mesosphere is relatively dry, the contribution to its local water vapor budget from launch vehicle exhaust may be significant.

[22] **Acknowledgments.** We thank the Flight Dynamics, Propulsion and Energy Systems Departments of the NASA Johnson Space Center for providing the shuttle ascent product and trajectory information. We also thank K. U. Grossmann for productive discussions, J. G. Cardon for assistance with data analysis and R. R. Conway for his leadership on the MAHRSI project. This work was supported by the NASA Office of Space Science.

## References

American Institute of Aeronautics and Astronautics (AIAA), *Atmospheric Effects of Chemical Rocket Propulsion*, 52 pp., New York, 1991.

Bernhardt, P. A., et al., Incoherent scatter from space shuttle and rocket engine plumes in the ionosphere, *J. Geophys. Res.*, *103*, 2239–2251, 1998.

Bodhaine, B. A., et al., On Rayleigh optical depth calculations, *J. Atm. Oceanic Tech.*, *16*, 1854–1861, 1999.

Conway, R. R., et al., Middle Atmosphere High Resolution Spectrograph Investigation, *J. Geophys. Res.*, *104*, 16,327–16,348, 1999.

Forbes, J. M., Upper atmosphere modifications due to chronic discharges of water vapor from space launch vehicle exhausts, in *Space Systems and Their Interactions with Earth's Space Environment*, edited by H. B. Garrett and C. P. Pike, *Progress in Astronautics and Aeronautics, 71*, 78–98, 1980.

Hedin, A., Extension of the MSIS thermosphere model into the middle and lower atmosphere, *J. Geophys. Res.*, *96*, 1159–1172, 1991.

Kellogg, W. W., Pollution of the upper atmosphere by rockets, *Space Sci. Rev.*, *3*, 275–316, 1964.

Körner, U., and G. R. Sonnemann, Global three-dimensional modeling of the water vapor concentration of the mesosphere-mesopause region and implications with respect to the noctilucent cloud region, *J. Geophys. Res.*, *106*, 9639–9651, 2001.

Kozlov, S. I., and N. V. Smirnova, Impact of the cloud formed during the space shuttle launch on the stratospheric ozone, *Int. Journ. Geomagnetism and Aeronomy*, *1*, 107–110, 1998.

Lieberman, R. S., et al., Comparison of mesospheric and lower thermospheric residual wind with High Resolution Doppler Imager, medium frequency, and meteor radar winds, *J. Geophys. Res.*, *105*, 27,023–27,035, 2000.

Lübken, F.-J., and U. von Zahn, Thermal structure of the mesopause region at polar latitudes, *J. Geophys. Res.*, *96*, 20,841–20,857, 1991.

Marti, J., and K. Mauersberger, A survey and new measurements of ice vapor pressure at temperatures between 170 and 250 K, *Geophys. Res. Lett.*, *20*, 363–366, 1993.

Mendillo, M., Ionospheric holes: A review of theory and recent experiments, *Adv. Space Res.*, *8*, 51–62, 1988.

Murad, E., et al., Visible light emission excited by interaction of space shuttle exhaust with the atmosphere, *Geophys. Res. Lett.*, *17*, 2205–2208, 1990.

Newman, P. A., et al., Chance encounter with a stratospheric kerosene rocket plume from Russia over California, *Geophys. Res. Lett.*, *28*, 959–962, 2001.

Roble, R. G., and E. C. Ridley, A thermosphere-ionosphere-mesosphere-electrodynamics general circulation model (time-GCM): Equinox solar cycle minimum simulations (30–500 km), *Geophys. Res. Lett.*, *21*, 417–420, 1994.

Ross, M. N., et al., Observation of stratospheric ozone depletion associated with Delta II rocket emissions, *Geophys. Res. Lett.*, *27*, 2209–2212, 2000.

Stevens, M. H., and R. R. Conway, Calculated OH $A^2\Sigma^+ - X^2\Pi$ (0,0) band rotational emission rate factos for solar resonance fluorescence, *J. Geophys. Res.*, *104*, 16,369–16,378, 1999.

Stevens, M. H., et al., PMCs and the water frost point in the Arctic summer mesosphere, *Geophys. Res. Lett.*, *28*, 4449–4452, 2001.

Summers, M. E., and D. E. Siskind, Surface recombination of O and $H_2$ on meteoric dust as a source of mesospheric water vapor, *Geophys. Res. Lett.*, *26*, 1837–1840, 1999.

Summers, M. E., et al., Implications of satellite OH observations for middle atmospheric $H_2O$ and ozone, *Science*, *277*, 1967–1970, 1997.

Vlasov, M. N., and V. V. Grushin, A model of global distribution of the exhaust gases from rocket engines in the upper atmosphere, *Cosmic Res.*, *34*, 30–35, 1996.

M. H. Stevens, C. R. Englert, and J. Gumbel, Code 7641, Naval Research Laboratory, 4555 Overlook Ave., SW, Washington, DC 20374, USA. (stevens@uap2.nrl.navy.mil)